Computers and Concrete, *Vol.15, No.4 (2015) 687-707*
DOI: http://dx.doi.org/10.12989/cac.2015.15.4.687

Time dependent finite element analysis of steel-concrete composite beams considering partial interaction

Maiga M. Dias, Jorge L.P. Tamayo *, Inácio B. Morsch and Armando M. Awruch

Department of Civil Engineering, Engineering School, Federal University of Rio Grande do Sul, Av. Osvaldo Aranha, 99-3°Floor, 90035-190, Porto Alegre, RS, Brazil

(*Received March 31, 2014, Revised October 31, 2014, Accepted February 11, 2015)*

Abstract. A finite element computer code for short-term analysis of steel-concrete composite structures is extended to study long-term effects under service loads, in the present work. Long-term effects are important in engineering design because they influence stress and strain distribution of the structural system and therefore contribute to the increment of deflections in these structures. For creep analysis, a rheological model based on a Kelvin chain, with elements placed in series, was employed. The parameters of the Kelvin chain were obtained using Dirichlet series. Creep and shrinkage models, proposed by the CEB FIP 90, were used. The shear-lag phenomenon that takes place at the concrete slab is usually neglected or not properly taken into account in the formulation of beam-column finite elements. Therefore, in this work, a three-dimensional numerical model based on the assemblage of shell finite elements for representing the steel beam and the concrete slab is used. Stud shear connectors are represented for special beam-column elements to simulate the partial interaction at the slab-beam interface. The two-dimensional representation of the concrete slab permits to capture the non-uniform shear stress distribution in the horizontal plane of the slab due to shear-lag phenomenon. The model is validated with experimental results of two full-scale continuous composite beams previously studied by other authors. Results are given in terms of displacements, bending moments and cracking patterns in order to shown the influence of long-term effects in the structural response and also the potentiality of the present numerical code.

Keywords: steel-concrete composite beams; viscoelasticity; creep; shrinkage; finite elements

1. Introduction

Steel-concrete composite structures are very attractive and widely used in civil engineering, allowing lower costs and improvements in the structural performance. A reinforced concrete slab is mechanically connected to the top flange of a rolled or fabricated steel beam, thereby forming a composite member stronger and stiffer than the steel beam acting on its own. Composite beams usually show partial composite actions, which is induced from the bond-slip deformation along the interface between the slab and the steel beam. In practical applications, it is not always possible or necessary to reach full shear connection in a composite beam. For instance, the number of shear connectors required to achieve full shear connection may be so large that there are difficulties in accommodating them in the beam, or on the other hand, the applied load carried by a beam may be safely sustained with less shear connectors than those required to reach full shear connection. The

*Corresponding author, Ph.D. Professor, E-mail: lpt.jorge@gmail.com

Copyright © 2015 Techno-Press, Ltd.
 ISSN: 1598-8198 (Print), 1598-818X (Online)

consideration of partial interaction represents an increase of lateral deflection and a decrease of resisting capacity and therefore the bond-slip effect should be accounted for in order to precisely evaluate the actual structural behavior of partially bonded composite beams.

Moreover, since concrete has the characteristics of shrinkage and creep, the final deflection of the composite beam under long-term load is generally several times the initial deflection, even under dead load only. This is due to the fact that creep and shrinkage of concrete may modify significantly stress distribution along time. Therefore, the rheological behavior of concrete is a very important factor in structural response. Factors influencing creep and shrinkage are strongly linked to the concrete age at loading, load duration, type of cement, geometry, relative humidity and temperature. The law of creep proposed by Bazant (1988) and the theory of solidification are still fairly used. There is a comprehensive body of literature relating to composite beams analysis under long-term effects. For instance, one-dimensional models based on beam-column elements are employed extensively, obtaining a good compromise between accuracy of solution and computational effectiveness (Macorini *et al.* 2006).

Within these one-dimensional formulations, one approach is based on using a single finite element composed of two parallel beams linked to each other through non-linear spring system acting along the beam axis. Alternatively, each of the parallel beams is modeled with its own set of beam-column elements, which are then linked using additional non-linear spring elements. Examples of these formulations are given in the works of Jiang *et al*. (2009) and Sakr and Sakla (2008) where the effects of creep and shrinkage of the concrete slab are considered only for uncracked concrete. The flexibility of the shear connection at the slab-beam interface is also considered in these models. In Gara *et al*. (2009), a beam finite element formulation for the long-term analysis of steel-concrete composite decks taking into account the shear lag in the slab and the partial shear interaction at the slab-beam interface is presented. The concrete is considered to be uncracked even under traction and behave in a linear viscoelastic fashion. In Valipour and Bradford (2009) and Hwang and Kwak (2013), formulations of 1D steel-concrete composite elements suitable for short-term loads that captures material nonlinearities and partial shear interaction are also presented. A very interesting analytical model of the behavior of continuous composite beam under service load is presented in Gilbert and Bradford (1995). Unlike the previous models, this model accounts for cracking of the concrete slab in the negative moment regions at each interior support as well as the time-dependent deformation caused by creep and shrinkage in the concrete slab.

Despite the success of the one-dimensional approach, there are some cases, such as when the structural response is affected by significant shear strains of the concrete slab in the horizontal plane, for which one-dimensional discretization is not suitable for the composite beam. This corresponds to the well-known phenomenon of shear-lag, which is complex to study for realistic composite beams even in the elastic range. Although the inclusion of the shear lag phenomenon in one-dimensional models is possible, it would require a more involved and complex formulation. In this way, research that includes the effect of shear stresses at slab is far more limited. Studies that include the shear lag phenomenon in the numerical modeling using a three dimensional approach, are given in Macorini *et al*. (2006) and Liu *et al*. (2013), for instance. In these cases, a two-dimensional representation of the slab is used, for which the strain distributions is typically non-uniform along a generic layer of the slab cross-section. Also, the use of layered shell elements for representing the concrete slab allow to capture concrete cracking patterns more realistically.

In this work, an elastic-plastic finite element model developed and implemented by Tamayo (2011) suitable for short-term loads was extended to consider long-term effects under service loads. For this purpose, creep and shrinkage strains are calculated according to the CEB-FIP90 model and

viscoelasticity theory is used. The slab of the steel-concrete composite beam is modeled with 8-node thick degenerated shell elements, the steel beam are modeled with 4-node thin plate shell elements and the connection between these two types of elements, given in the real structure by stud connectors, is provided by a three-dimensional 2-node beam-column element, which enables flexible or rigid coupling between the nodes of each part. The numerical model is able to trace the complete non-linear response of composite beams under long-term loads, non-uniform shear stress distribution and realistically cracking patterns at the concrete slab are also obtained. Work is undergoing in order to include prestressed tendons at the concrete slab for modeling long-span bridges. Validation of the numerical model is demonstrated by reproducing two full-scale continuous composite beams tested for a period of 340 days. Previous studies have dealt with these examples, but a proper three-dimensional numerical model has not been addressed before and therefore not cracking patterns have been reported. Also, the model is able to calculate bending moments along the beam axis showing clearly the influence of the long-term effect in the final structural response.

2. Elasto-plastic constitutive model for reinforced concrete, steel beam and shear connectors

Concrete in compression is modeled using the associated theory of plasticity; a modified Drucker-Prager yield criterion (Tamayo *et al*. 2014) is used in this work. Due to nonlinear hardening behavior, this yield criterion defines an initial yield surface at effective stress equal to $\sigma_o = 0.3 f_c$ (which is considered the beginning of the plastic deformation), being f_c the concrete compression strength and a limit surface which separates nonlinear state from a perfect elasto-plastic one as shown in Figs. 1(a)-(b).

The stresses and strains are to be calculated according to a local orthogonal Cartesian coordinate system ($x'y'z'$) defined at sampling points in order to easier deal with the shell assumption of zero normal stress. The normal direction, which is taken perpendicular to the current layer surface, is

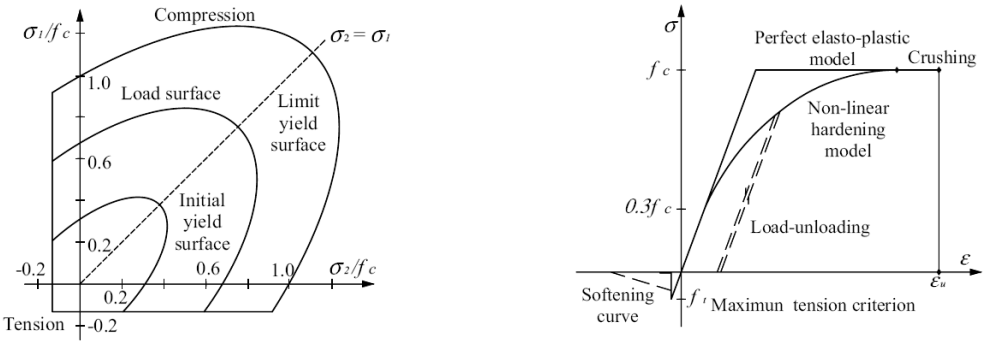

(a) Two-dimensional criterion in principal plane (b) One-dimensional representation

Fig. 1 Concrete model

obtained by the cross product of two tangential directions at the current sampling point (Tamayo

2011). Because the concrete slab lies in the horizontal global plane XY, the directions of this local coordinate system coincide with those of the global coordinate system (XYZ) and the yield criterion is defined by:

$$f(\sigma)=\left\{1.355\left[\left(\sigma_{x'}^2+\sigma_{y'}^2-\sigma_{x'}\sigma_{y'}\right)+3\left(\sigma_{x'y'}^2+\sigma_{x'z'}^2+\sigma_{y'z'}^2\right)\right]+0.355\sigma_o\left(\sigma_{x'}+\sigma_{y'}\right)\right\}^{1/2}=\sigma_o \qquad (1)$$

where σ_o is the effective stress. In addition, the associated rule is defined as:

$$d\varepsilon_{ij}^p=d\lambda\frac{\partial f(\sigma)}{\partial\sigma_{ij}}=\frac{\{a\}^T[D]_e}{H'+\{a\}^T[D]_e\{a\}}\{d\varepsilon\}\frac{\partial f(\sigma)}{\partial\sigma_{ij}} \qquad (2)$$

with

$$\{a\}^T=\left[\partial f/\partial\sigma_{x'}\quad \partial f/\partial\sigma_{y'}\quad \partial f/\partial\sigma_{x'y'}\quad \partial f/\partial\sigma_{x'z'}\quad \partial f/\partial\sigma_{y'z'}\right] \qquad (3)$$

where $[D]_e$ is the elastic constitutive matrix of the material, $\{d\varepsilon\}$ is a vector containing the increments of strain components, H' is the hardening parameter, considered as the slope of the one-dimensional curve shown in Fig. 1(b), in which the hardening rule is defined and $d\lambda$ is the plastic multiplier. In this work, the curve known as "Madrid Parabola" is adopted and is defined in the following way:

$$\sigma_o=H'\left(\bar{\varepsilon}_p\right)=E_c\bar{\varepsilon}_p+\left(2E_c{}^2\varepsilon_o\bar{\varepsilon}_p\right)^{\frac{1}{2}} \qquad (4)$$

where E_c is the elastic modulus of concrete, ε_o represents the total strain at maximum compressive stress f_c (usually 0.002) and $\bar{\varepsilon}_p$ is the effective plastic deformation obtained from a work hardening hypothesis. The elasto-plastic constitutive relation is expressed in the following differential form:

$$\{d\sigma\}=[D]_{ep}\{d\varepsilon\}=\left\{[D]_e-\frac{[D]_e\{a\}[D]_e\{a\}^T}{H'+\{a\}^T[D]_e\{a\}}\right\}\{d\varepsilon\} \qquad (5)$$

Finally, the crushing condition is given by:

$$1.355\left(\varepsilon_{x'}^2+\varepsilon_{y'}^2-\varepsilon_{x'}\varepsilon_{y'}\right)+1.01625\left(\gamma_{x'y'}^2+\gamma_{x'z'}^2+\gamma_{y'z'}^2\right)+0.355\varepsilon_u\left(\varepsilon_{x'}+\varepsilon_{y'}\right)=\varepsilon_u^2 \qquad (6)$$

where ε_u represents the ultimate strain extrapolated from experimental test whose values ranges from 0.003 to 0.0045. On the other hand, the response of concrete under tensile stresses is assumed to be linear elastic until the fracture surface is reached and then, its behavior is characterized by an orthotropic material. The cracking is governed by a maximum stress criterion. Cracks are assumed to occur in planes perpendicular to the direction of the maximum tensile stress as soon as this stress reaches the specified concrete tensile strength f_t. After cracking has occurred the elastic modulus

E_c and Poisson´s ratio G are assumed to be zero in the direction perpendicular to the cracked plane, and a reduced shear modulus is employed. The adherence between the concrete and the reinforcing bars is responsible for the capacity of the stress retention of the cracked concrete. That is, due to bond effects, cracked concrete carries, between cracks, a certain amount of tensile force normal to the cracked plane. This effect is known a tension stiffening effect and is considered through a relationship between the strain and the stress normal to the cracking plane direction as shown in Fig. 2(a), where ε_{ct} is the strain associated with f_t and ε_{tm} is the maximum strain for $0.5 \leq \alpha \leq 0.7$. The normal stress σ_i is determined from a known value of strain ε_i. In the case of simple concrete or for concrete far away from the influence zone of the reinforcing bars, the previous diagram (or relationship) is also used (Povoas 1991) in conjunction with the fracture energy of the material G_f (0.25-0.58 N/cm) and the representative thickness h of the concrete specimen in order to guarantee the objectivity of the finite element solution. In all examples presented in this work, firstly a sensitivity analysis has been carried out in order to prove mesh independence of the finite element results. In addition, the model considers the opening and closure of cracks and in the post-cracking stage, a fixed crack orientation is assumed, such orientation being orthogonal to the direction of the maximum principal stress that first exceeds the concrete tensile strength.

The reinforcing bars in the concrete slab are modeled as a membrane layer of equivalent thickness oriented according to the actual reinforcement direction, following the behavior of a one–dimensional elasto-plastic material with a yielding stress equal to σ_o, a constant elastic steel modulus E_s and a tangential elastic modulus $E_{s'}$, as shown in Fig. 2(b). Further details of the reinforced concrete constitutive model can be found in Tamayo (2011) and Tamayo *et al*. (2014).

In relation to the steel beam, as thicknesses of the web and flanges are considered to be smaller than that of the concrete slab, the theory of thin plates is used for modeling these parts of the structure besides a plane stress assumption. The multiaxial state of stress in the steel beam follows

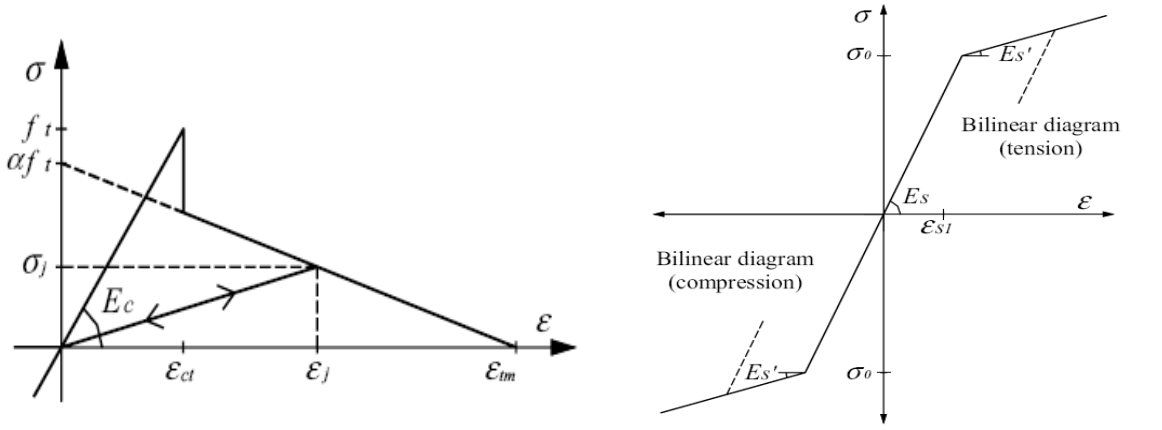

(a) Tension stiffening model

(b) Bilinear stress-strain relationship for reinforcing bars

Fig. 2 Constitutive model for concrete in traction and steel reinforcement constitutive law

the Von Mises yield criterion with a hardening law defined by the one-dimensional bilinear curve

shown in Fig. 2(b). However, because service loads are considered in this work, the whole steel beam behaves in a linear elastic fashion. The connection system at the slab-beam interface is discrete and is represented by three-dimensional beam-column elements located in the finite element mesh according to its real positions. The behavior in the element is dictated by the non-linear relationship of the shear force in the connector versus the slip that takes place at the slab-beam interface. Here, the exponential law proposed by Razaqpur and Nofal (1989) is used to represent this behavior along the longitudinal and transverse direction of the composite beam, whereas a rigid or flexible connection can be assigned in other directions. The shear stiffness is non-linear since the beginning of loading and the constitutive law is defined in the following manner:

$$F_\beta = c\left(1 - e^{-ds_\beta}\right) \tag{7}$$

where F_β and s_β are the shear force acting in the shear connector and the slip associated in the β direction, respectively. The constant *c* and *d* define the shape of the constitutive curve and are determined by experimental fitting obtained from push-out test results. The tangent to this curve defines the current stiffness of the shear connector to be used in the element stiffness matrix. Both steel and connection do not exhibit rheological phenomena, hence the same laws are considered for short- and long-term analyses. Explicit expressions for the stiffness of the steel beam and shear connectors can be found in Tamayo (2011). Then, the reader is referred to that reference for more details.

3. Finite element formulation

The finite element employed for the concrete element is a degenerated shell finite element based on the theory of thick plates. The element is composed of several layers through thickness in order to capture nonlinearity variation due concrete cracking and non-linear compression behavior. It is assumed that the layers, normal to the surface, remain straight after deformation. Also the strain energy corresponding to the stress component perpendicular to the finite element mid-surface is disregarded. A quadratic finite element with eight nodes and five degrees of freedom at each node (three translations and two rotations) is adopted. The reinforcement mesh within the concrete slab is defined in its real position through thickness as another layer of equivalent thickness and with steel properties. The thickness of this layer is calculated since the current area of the reinforcing bars for the considered effective width (Dias 2013). Perfect adherence is also considered between reinforcing bars and the surrounded concrete. In a time dependent analysis, it is important to properly account for the development of the time-dependent strains in the structure such as creep and concrete shrinkage. Thus, the element stress-strain relationship should properly consider those effects (Dias 2013).

The steel beam was modeled using a plane shell element obtained from the assemblage of a membrane element with drilling degree of freedom and a thin plate element (Tamayo *et al*. 2014). Introduction of the drilling degree of freedom notably improves the element behavior under bending. Inelastic behavior of the steel is considered by using a five point integration rule through thickness. A bilinear finite element with four nodes and six degrees of freedom at each node (three translations

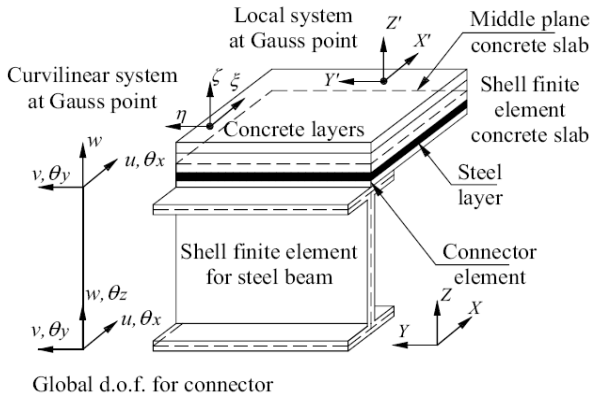

Fig. 3 Assembly of finite elements for composite beam made of steel, concrete and shear connectors

and three rotations) is adopted. The stud shear connectors are represented by a three-dimensional beam-column element with special characteristics to take into account nonlinearity of the shear force in the transversal and longitudinal directions. The connection system, generally made of mechanical studs, is modeled by introducing an interaction law between the two nodes of the connector element, one belonging to slab middle plane and the other to the middle plane of the top flange of the steel beam. For details about the finite element formulation of these elements, the reader is referred to the work of Tamayo (2011), Dias (2013) and Tamayo *et al*. (2014).

In Fig. 3 is depicted a short element of steel-concrete composite beam after assembly. Determination of stiffnesses and internal forces at the element level and the assemble procedure are performed as usually and they have been already presented in some text books (Smith *et al*. 2014). As it was stated before, in Fig. 3, the local coordinate system at each sampling point of each layer at the concrete slab follows the directions of the global coordinate system for the present case.

4. Solidification theory – creep concrete

Because it is numerically expensive to store all time-history of each of the involved variables, the formulation proposed by Bazant and Prasannan (1988), employing a creep law without aging, was adopted in the present work. A Kelvin chain-based rheological model was used, with time-independent elastic and viscous parameters, as in the classical linear viscoelastic theory. The total strain of a Kelvin chain at instant t due to a load applied at time t_0 is given by:

$$\gamma(t-t_0)=\sum_{\mu=1}^{N}\frac{1}{E_\mu}(1-e^{-(t-t_0)/\tau_\mu}) \tag{8}$$

where E_μ, $\tau_\mu=\eta_\mu/E_\mu$ and η_μ are the elastic modulus, retardation time and viscosity of the μ-th component of the Kelvin chain, respectively and N is the total number of elements in the Kelvin chain. Eq. (8) is known as Dirichlet series, which may be fitted to various creep curves. Proper determination of retardation times is needed for curve fitting (Bazant, 1988). In this work the following expression for retardation times was adopted:

$$\tau_\mu = \tau_1 10^{\mu-1} \quad \mu = 1,2,...,N \quad \rightarrow \quad \tau_1 = 0.01 t_0 \quad \tau_N \geq 0.5 t_{max} \tag{9}$$

It is necessary to choose time steps in order to determine $1/E_\mu$. It is more effective to keep constant time steps using a logarithmic scale $(t - t_0)$ where t_0 is the instant at which the first load is applied or the instance where the first strain is imposed to the structure (Bazant 1988). Then, it is needed to choose the initial step (t_0, t_1), and then, t_r is generated successively until the final time, with the following expression:

$$t_{r+1} - t_0 = 10^{1/m}(t_r - t_0) \qquad \rightarrow \quad t_1 - t_0 = 0.1 t_0 \tag{10}$$

where *m* (number of steps per decade) may be adopted with a value around 10 to obtain a good accuracy. In the Solidification Theory proposed by Bazant and Prassanan (1988), the creep function for a material with aging, like concrete, is given by the following expression:

$$J(t,t_0) = \frac{1}{E_c(t_0)} + \frac{\gamma(t,t_0)}{V(t)} \tag{11}$$

where $E_c(t_0)$ is the elasticity modulus at the load application instant (t_0) in MPa, $V(t)$ is the solidified concrete volume (which is taken as an aging function) and $\gamma(t,t_0)$ is the Kelvin chain strain. According to the Comité Euro-International du Béton (1990), the creep function is given by:

$$J(t,t_0) = \frac{1}{E_c(t_0)} + \frac{\varphi_0(t_0)\varphi_1(t,t_0)}{E_c(28)} \tag{12}$$

where $E_c(28)$ is the elasticity modulus at 28 days, $\varphi_0(t_0)$ is the ideal creep coefficient and $\varphi_1(t,t_0)$ is a function of time that describes creep development after loading. A comparison between both formulations for the creep function $J(t,t_0)$, expression (11) and (12), gives:

$$\gamma(t,t_0) = \varphi_1(t,t_0) \quad ; \quad V(t) = \frac{E_c(28)}{\varphi_0(t_0)} \tag{13}$$

where:

$$\varphi_1(t,t_0) = \left[\frac{(t-t_0)}{\beta_H + (t-t_0)} \right]^{0.3} \tag{14}$$

being β_H a constant given by the CEB-FIP90 model.

With this comparison, the parameters E_μ can be obtained by evaluating the function $\varphi_1(t,t_0)$ given in the CEB-FIP90 model at *L* specified points. The following system of linear equations is obtained by employing the least squares method:

$$[A]\{X\} = \{B\} \rightarrow A(i,j)X(j) = B(i) \qquad i, j = 1,2,...,N \tag{15}$$

$$A(i,j)=\sum_{k=1}^{L}\left[1-e^{-(t-t_0)_k/\tau_i}\right]\left[1-e^{-(t-t_0)_k/\tau_j}\right] \tag{16}$$

$$B(i)=\sum_{k=1}^{L}\varphi_1(t,t_0)_k\left[1-e^{-(t-t_0)_k/\tau_i}\right] \tag{17}$$

$$X(j)=1/E_j \tag{18}$$

Then, solving the system of equations given in Eq. (15), the Kelvin chain parameters E_μ can be obtained. Shrinkage strains were obtained using directly the CEB-FIP90 model code. In Bazant and Oh (1984) good match between numerical and experimental results in the prediction of deflections was found for simply and doubly reinforced concrete beams when the creep coefficient is considered to be larger in traction than that for compression stresses (approximately three times larger). Later, Alwis *et al*. (1994) also obtained good results for the same set of experimental beams using the same creep coefficient in traction and compression, but including the effect of concrete shrinkage in the numerical modeling. As in the works of Macorini *et al*. (2006) and Sakr and Sakla (2008), in this work, the creep compliance function and the shrinkage strain are assumed to be the same in traction and compression and are evaluated according to the CEB-FIP90 model.

5. Numerical algorithm

A finite element constant or tangent stiffness formulation, coupled with a step-by-step integration scheme in the time domain, is developed to analyze steel-concrete composite beams. Within each time step, an incremental load procedure, with an iterative approach to solve of the equilibrium equations for each load increment, is used. The entire time period, for which the response history of the structure is to be analyzed, is divided into a number of time steps, Δt_1, Δt_2, Δt_3,…, Δt_n. It is assumed that changes in the external nodal loads, if any, occur only at the beginning or at the end of a time step. During a time step, the external loads are assumed to remain constant. The increment of the external nodal loads at any particular time, may be subdivided into a number of load steps to follow the non-linear response of the structure in more detail. For a given force $R(t_i)$, the increment in the external nodal vector at time t_i could be divided into n load steps ΔR_j $(j=1,2,...,n)$. An iterative approach is then used to solve for each load step and the increments in the field variables (strains and stresses) are added to the previous total values to give the current stress and strain states of the structure. The basic steps of the numerical method of analysis are presented below (Dias 2013).

1. Read all data related to the geometry of the structure and input data for constitutive relations and time-dependent material properties, type of layers and element properties.
2. Read the load control data for the current time t_i and time step Δt_i ($\Delta t_i = t_{i+1} - t_i$). Form the applied load vector $R(t_i)$ for time t_i. Divide this vector in a given number of load steps to obtain the load vector for each load step of the current increment.
3. Start the iterative solution procedure for this load step.
4. Form the element stiffness matrices and assemble the structural stiffness matrix. This step may be performed only for the first iteration of each load step.
5. Solve the equilibrium equations to obtain nodal displacements incremental vector. Add this

vector to the previous total displacement vector to obtain the current total nodal displacement vector in the global coordinate system. Check convergence if the displacement norm is used.

6. Calculate for each element the local deflection increment and the corresponding strain and stress increments. Update material matrix, calculate current total strain and stress components, and calculate the element resisting forces based on the current state.

7. Transform all the element resisting forces to the global coordinate system and assemble the current structural internal resisting force vector. The unbalanced force vector is given by subtracting the total applied external load from the internal resisting force vector. Check convergence if the force norm is used.

8. If convergence has not been obtained, go back to step 4 and repeat steps 4 to 7 until convergence is achieved or the maximum number of iterations allowed is reached. If the equilibrium state has been found, go to step 9, or, if the solution diverges, stop calculations.

9. If this is not the last load step for the current time, go back to step 2 and repeat steps 2 to 8 until the solution is obtained for all the specified load steps. When the last load step was reached, go to the next step.

10. Calculate the material properties at the end of the time steps, i.e., for time t_{i+1}. For each element the creep and shrinkage strains are calculated and the stresses are assumed to be constant during the load step. The equivalent nodal loads for each element are calculated by considering these strains as initial strains and then they are assembled into the structural load increment vector. Go to step 2 and repeat steps 2 to 8.

11. If time t_i is the last time the analysis is finished, otherwise go back to step 2 and continue the analysis for the next time step.

Most of the steps in the algorithm are standard procedures used in any computer program employing the finite element method. The manner in which the time dependent vector is calculated (step 10) is presented in section 5.1. The determination of the state in the concrete layers, mentioned in step 6, is explained in detail by Tamayo *et al*. (2014) and only a brief comment is given in section 5.2.

5.1 Solution procedure for creep and shrinkage effects

Assume all load changes to occur at the beginning of the time step. By solving the equilibrium equations for these load changes, all the field variables (nodal displacement vector, strain and stress) are known for all elements. Creep and shrinkage laws are also specified. A step-by-step integration scheme in the time domain is employed to analyze the effects of time-dependent phenomena. The non-linear response of the structure is traced over a time period by dividing this time period into a number of smaller time steps. An initial strain approach (Dias 2013) is adopted to determine the response of the structure due to the time-dependent strain increments occurring during a time step. The procedure is presented below for time step Δt_i ($\Delta t_i = t_{i+1} - t_i$).

At the beginning of the time step *i*, the stress components $\{\sigma\}_i$ are known, as well as the stress components $\{\sigma\}_{i-1}$ obtained at the previous step. At the first time step, components of stress increments vector, $\{\Delta\sigma\}_{i-1}$ are equal to zero. The stress increment for the time step *i* is calculated with $\{\Delta\sigma\}_i = \{\sigma\}_i - \{\sigma\}_{i-1}$ and the following algorithm is used to calculate equivalent nodal forces due to long-term effects:

- For each element *e*, a load vector due to creep and shrinkage effects with contribution of all the Gauss points *g*, considering all layers adopted in the normal direction to the surface of the concrete slab, is computed, with:
- For $e = 1\ldots m$ (where *m* is the total number of finite elements in the concrete slab);
- For $g = 1\ldots p$ (where *p* is the total number of Gauss points in each element):

1. In the element *e*, for Gauss point *g*, the shrinkage strain for time step *i* is given by:

$\{\varepsilon_{cs}\}_{(g,e,i)}$ (CEB – FIP90)

2. Strain increment due to shrinkage is given by:

$$\{\Delta\varepsilon_{cs}\}_{(g,e,i)} = \{\varepsilon_{cs}\}_{(g,e,i)} - \{\varepsilon_{cs}\}_{(g,e,i-1)}$$

3. Functions $\varphi_o(t_0)$ and $V(t)$ are computed employing CEB-FIP90 formulation.
4. Creep strain is quantified by the sum of the strain of each Kelvin chain element:
- For $\mu = 1,\ldots,N$, being *N* the total number of Kelvin chain elements:

$$\{\varepsilon^*_\mu\}_{(g,e,i)} = [D_\mu]^{-1}_{(g,e,i)}\{\Delta\sigma\}_{(g,e,i)} + \{\varepsilon^*_\mu\}_{(g,e,i-1)}\left(e^{-\Delta t_i/\tau_\mu}\right)$$

$$\{\Delta\varepsilon_\mu\}_{(g,e,i)} = \sum_{\mu=1}^{N}\{\varepsilon^*_\mu\}_{(g,e,i)}\left(1-e^{-\Delta t_i/\tau_\mu}\right) + \{\Delta\varepsilon_{cs}\}_{(g,e,i)}$$

where $[D_\mu]^{-1}$ is the inverse of the isotropic constitutive matrix evaluated with an elasticity modulus equal to $E_\mu V_{i+1/2}/\lambda_\mu$; being $\lambda_\mu = \left(1-e^{-\Delta t_i/\tau_\mu}\right)/\left(\Delta t_i/\tau_\mu\right)$.

5. Matrix $[D]^*_{(g,e,i)}$ is evaluated with the effective modulus $E^*_{(g,e,i)}$, which is given by:

$$1/E^* = \frac{1}{E_{i+1/2}} + \sum_{\mu=1}^{N}\frac{1-\lambda_\mu}{E_\mu V_{i+1/2}}$$

where $i+1/2$ is the middle of the interval (t_i, t_{i+1}). Constitutive matrix $[D]^*$ is given by:

$$[D]^* = \begin{bmatrix} \frac{E^*}{1-\nu^2} & \frac{\nu E^*}{1-\nu^2} & 0 & 0 & 0 \\ \frac{\nu E^*}{1-\nu^2} & \frac{E^*}{1-\nu^2} & 0 & 0 & 0 \\ 0 & 0 & G & 0 & 0 \\ 0 & 0 & 0 & G & 0 \\ 0 & 0 & 0 & 0 & G \end{bmatrix}$$

with $G = E^*/2(1+\nu)$ and ν is the coefficient of Poisson.

6. The equivalent element force vector is formed by summation of each Gauss point *g* contribution, being *p* the total number of Gauss points:

$$\{\Delta R\}_{(e,i)} = \sum_{g=1}^{p} \int_{V_e} [B]^T_{(g,e)} [D]^*_{(g,e,i)} \{\Delta \varepsilon^*\}_{(g,e,i)} \, dV_e$$

7. The global force vector due to creep and shrinkage at time step *i*, $\{\Delta R\}_i$, is assembled, considering the contribution of each load vector at element level;

8. At the end of the time step, the elasticity modulus is updated by the effective modulus E^*.

5.2 States of stress and strain determination in concrete layers

The behavior of concrete is characterized by an elasto-plastic constitutive law besides a cracking monitoring algorithm. A step-iterative approach is adopted to analyze the nonlinear behavior with a series of piecewise linear solutions. The stress increment vector in any concrete layer is obtained through the material constitutive matrix and the mechanical strains. These strains are obtained by subtracting the total strains from the non-mechanical ones due to creep and shrinkage (Dias 2013).

6. Numerical applications

6.1 Series C beams tested by Jaccoud and Favre (1982)

The RILEM Technical Committee TC 114 suggests, for long-term analysis benchmarks, the Series C beams, experimentally tested by Jaccoud and Favre (1982). Main characteristics of these beams are shown in Fig. 4(a). A sketch of the layers division is shown in Fig. 4(b), where the actual thickness of the concrete slab and the actual position of steel layers are indicated at the left side, while the position and thickness of the normalized steel layers are located at the right side. The slab thickness is normalized within a range of -1 to +1. The angle refers to the longitudinal reinforcement direction. Each reinforced concrete beam was subjected to five different permanent load levels. In Table 1 the phases of each structure in the test, according with the applied load, are presented. Besides the self-weight of the structures, the beams were subjected to two equidistant loads from its center. Table 2 shows the values of the properties used in the analysis, for each beam. These values are within the minimum and maximum range displayed on the original report.

The load was applied at 28 days and kept constant up to 528 days, except for the C11 beam which was maintained for a period of only 365 days. Due to symmetry, just the half beam was modeled with 96 8-node concrete shell elements. The number of equations is 480. The self-weight was treated as a distributed load of 3.924kPa, and was applied as a pressure load at the upper surface of the beams. The concentrated load was applied at the center of the beam width. The cement was considered with normal hardening at a temperature of 20℃. The relative humidity adopted was 55%

Table 1 Beams state after loading by Jaccoud and Favre (1982)

Beam	Load P (kN)	State
C11	5.77	Homogeneous
C12	12.19	First cracks
C13	18.61	cracked
C14	25.04	Advanced cracks
C15	31.45	Service limit

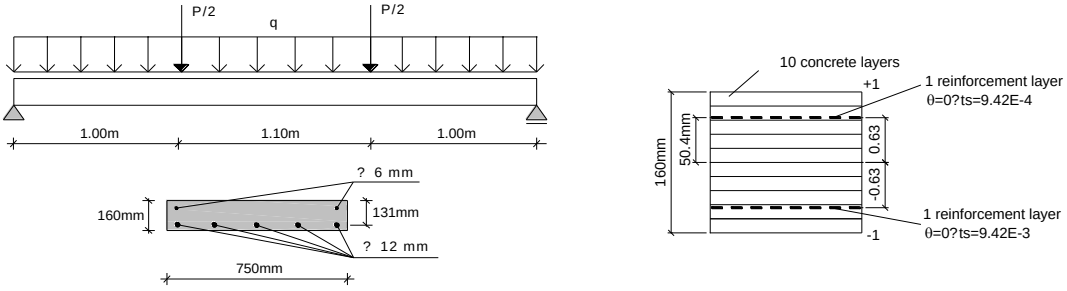

(a) Geometry of series C beams (b) Layers of series C beams

Fig. 4 Geometry of series C beams

Table 2 Material properties of series C beams

Material	Properties			
Steel	Young′s modulus (MPa)		E_s	200000
Φ 6mm	Yield stress (MPa)		f_y	580
Steel	Young′s modulus (MPa)		E_s	200000
Φ 12mm	Yield stress (MPa)		f_y	580
Concrete	Young′s modulus (MPa)	C11, C13	E_{28}	27500
		C12, 14	E_{28}	28300
		C15	E_{28}	28500
	Compressive strength (MPa)	C11, C13	f_c	26.6
		C12, 14	f_c	27
		C15	f_c	27.4
	Tensile strength (MPa)	C11, C13	f_t	2.25
		C12, 14	f_t	2.55
		C15	f_t	2.73
	Coefficient of Poisson		ν	0.2
	Ultimate compression strain (‰)		ε_u	3.5
	Ultimate tension strain (‰)		ε_{tm}	3
	Parameter for tension stiffening		α	0.5

for beams C11 and C13, 50% for beams C12 and C14 and 60% for beam C15. A Kelvin chain with 4 parameters was used and values of elastic modulus and retardation time for each element of the Kelvin chain are: E_1=8.56, τ_1=0.28; E_2=8.78, τ_2=2.8; E_3=4.03, τ_3=28; E_4=2.34, τ_4=280.

The creep coefficient and shrinkage strain for all studied beams were validated with the experimental results presented by Jaccoud and Favre (1982) for a period of about 500 days (not shown here). The evolution of the mid-span deflection at early ages is compared with the experimental measures for each load level in Fig. 5. It shows that the prediction algorithm was able

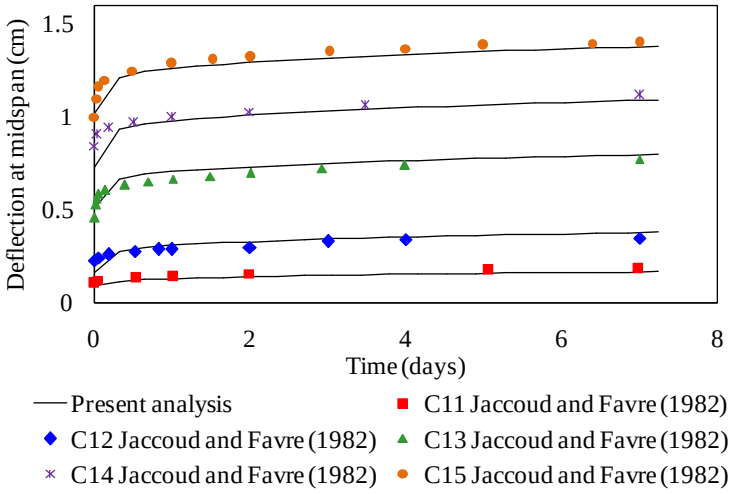

Fig. 5 Deflection at midspan for series C beams, immediately after loading

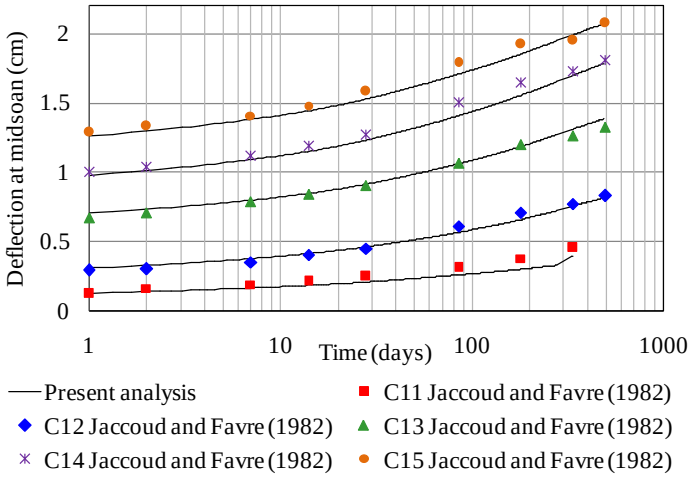

Fig. 6 Long-term deflection at mid-span for series C beams

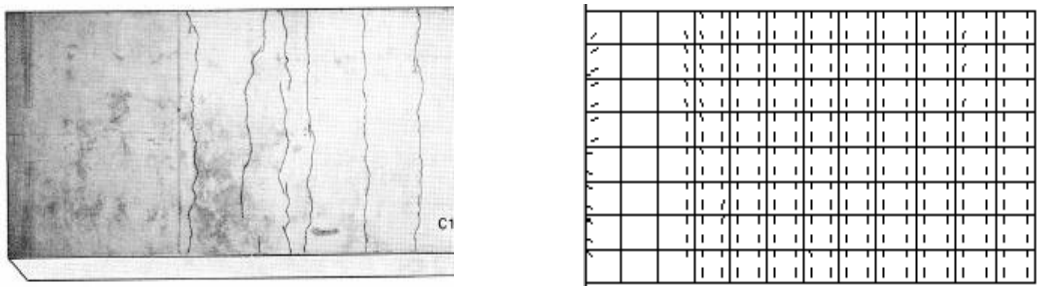

a) Font: Jaccoud and Favre (1982) b) Present analysis

Fig. 7 Cracks on the bottom of half beam C15 due to a load acting during 510 days

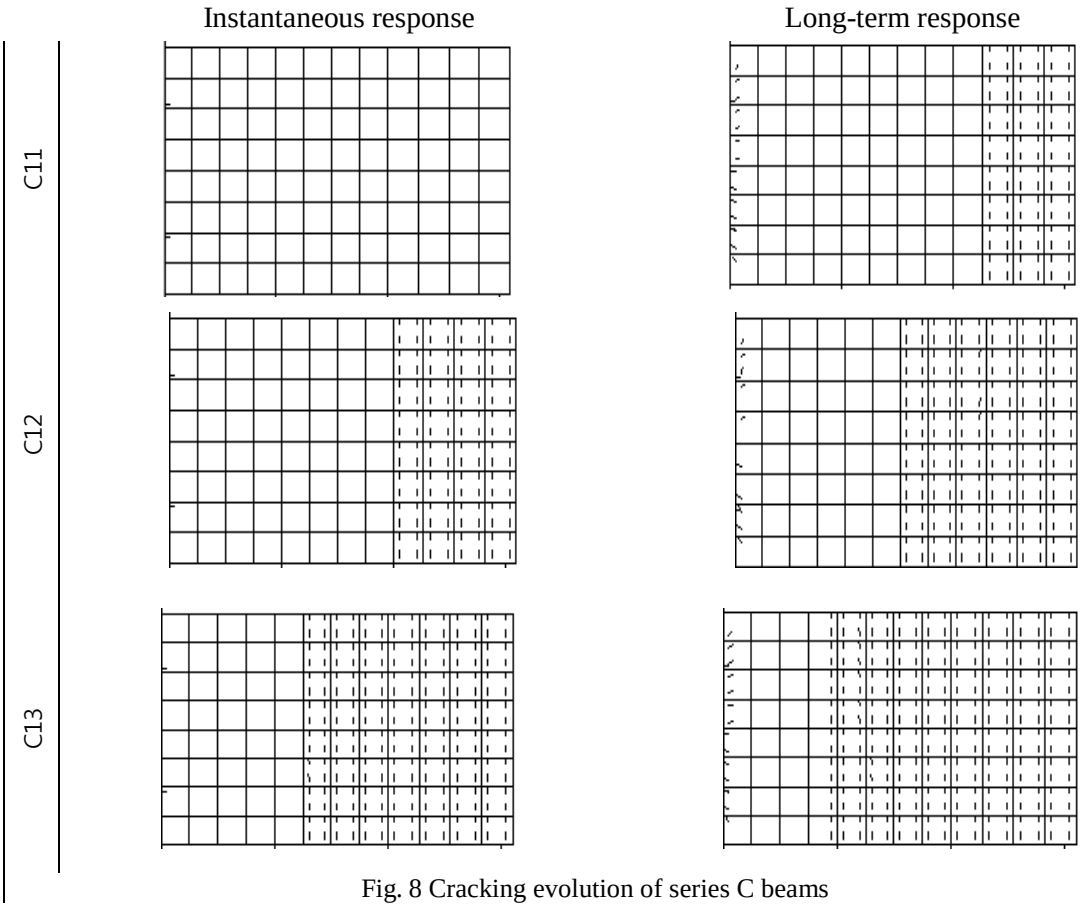

Fig. 8 Cracking evolution of series C beams

to obtain a good approximation between experimental and numerical results, even for early age concrete. In Fig. 6, results for the load acting for periods of 340 and 500 days are presented. A good approximation between experimental and numerical results is also observed.

The crack pattern in the bottom of C15, obtained by the experimental report, 510 days after loading, is shown in Fig. 7(a). The crack pattern obtained by the current analysis, where the traces indicate the cracking and its orientation, can be visualized in Fig. 7(b). It shows a good agreement with the mapping of cracks observed in the experimental work. As cracking is the main concern of the analysis, in Fig. 8, the cracking evolution is presented for beams C11, C12 and C13. The first column corresponds to the instantaneous response ($t_0 = 28$ days) and the second column, to long-term response ($t_f = 510$ days, except C11 beam with $t_f = 365$ days). It is possible to verify the level of cracking shown in Table 1

In relation to the computational time needed for analyzing the series of C beams, the algorithm was able to predict crack patterns similar to those obtained in the experimental tests by using 256 time steps in the analysis; being the average time of computation approximately 21 minutes for each beam. The analysis was carried out in AMD Athlon X2 processor with 2.7 GHz of speed. A tolerance equal to 1% in the norm of unbalanced forces was used for all examples presented here.

6.2 Continuous steel-concrete composite beams of two spans tested by Gilbert and Bradford (1995)

Two composite beams, both having two spans were experimentally tested by Gilbert and Bradford (1995) for a period of 340 days. Beams characteristics are shown in Fig. 9. The first beam (B1) was submitted to a self-weight load equal to 1.92kN/m, and the second beam (B2) supported, besides its self-weight load, a superimposed load of 4.75kN/m. The self-weight was

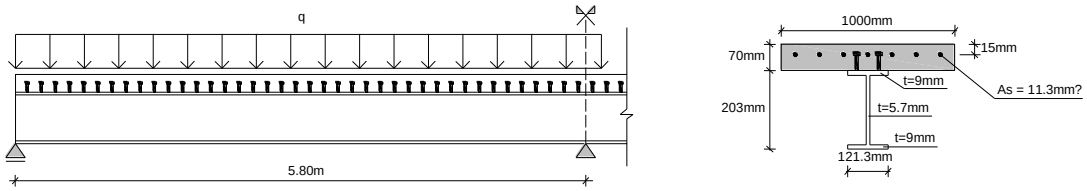

a) Longitudinal view b) Transversal section

Fig. 9 Geometry of continuous steel-concrete composite beam

Table 3: Material properties of continuous steel-concrete composite beams

Material	Properties		
Structural steel	Young′s modulus (MPa)	E_s	200000
	Yield stress (MPa)	f_y	280
	Ultimate stress (MPa)	f_u	350
	Coefficient of Poisson	v	0.3
	Ultimate strain (%)	ε_u	25
Reinforced steel	Young′s modulus (MPa)	E_s	200000
	Yield stress (MPa)	f_y	280
	Ultimate stress (MPa)	f_u	350
	Coefficient of Poisson	v	0.3
	Ultimate strain (%)	ε_u	25
Concrete	Compressive strength (MPa)	f_c	27
	Young′s modulus (MPa)	E	22000
	Tensile strength (MPa)	f_t	3
	Coefficient of Poisson	v	0.2
	Ultimate compression strain (‰)	ε_u	1
Shear connector	Spacing (mm)	s	145
	Diameter x height (mm)	dxh	9 x 50
	Row number		2
	Constant 1 (kN)	a	32
	Constant 2 (mm^{-1})	b	4.75

applied as a pressure load at the beams upper surface. The superimposed load of beam B2 was applied along its length as a pressure load acting in a central width of 60.65mm. Table 3 shows the values of the properties used in these examples.

According to Gilbert and Bradford (1995), for the final period, the creep coefficient measured was 1.68, whereas the shrinkage strain was 0.00052. Due to uncertainty of the age of loading, two loading times of 3 and 7 days were considered in the analysis following the study of Chaudhary *et al*. (2007). A Kelvin chain with 5 parameters was used. Values of the elasticity modulus and retardation time for each element of the Kelvin chain are: E_1=23.47, τ_1=0.03; E_2=24.03, τ_2=0.3; E_3=11.52, τ_3=3; E_4=6.14, τ_4=30; E_5=2.40, τ_5=300 for a loading time of 3 days and E_1=18.21, τ_1=0.07; E_2=18.62, τ_2=0.7; E_3=8.94, τ_3=7; E_4=4.64, τ_4=70; E_5=2.16, τ_5=700 for a loading time of 7 days.

Properties of stud shear connectors, dimensions and arrangement were based on Jiang *et al*. (2009) studies. These authors used the same connector formulation employed by Tamayo (2011) and adopted a maximum value of slip equal to 1.25mm. In this work, a tangential formulation was used for the evaluation of the connector stiffness.

Using symmetry, only half of the structure was modeled. As it is depicted in Fig. 10(a), the finite element mesh is composed of 287 8-node degenerated shell elements for modeling the concrete slab, 369 4-node shell elements for modeling the steel beam and 80 2-node beam-column elements for representing the shear connectors. The total number of degree of freedoms in the model is 7310. For the concrete slab layered model, seven concrete layers of the same thickness and one steel layer, representing the reinforcement, were used. Two additional meshes composed of 1040 and 1495 elements were considered for the concrete slab in order to prove mesh objectivity. Almost identical results were obtained for all meshes.

In Fig. 10(b) the instantaneous and final deformed meshes for beam B2 and also the considerable slip that takes place at the slab-beam interface are shown. The mid-span deflections obtained by the present analysis were compared with experimental and theoretical results obtained by Gilbert and Bradford (1995). These authors considered a one-dimensional analytical model using the aged-effective modulus method for including long-term effects. Mid-span deflections for both loading times are shown in Fig. 11.

As it can be seen, the differences for both loading times are small, being results for the loading time of 3 days closer to the experimental tests. Mid-span deflection for beams B1 and B2 are largely increased due to long-term effects during 340 days of sustained load from values of 0.1 cm and 0.35 cm to 0.4 cm and 0.8 cm, respectively.

The self-weight load, applied at 3 days, did not cause cracks in the beam B1, and the cracking process began after 38 days, approximately. Due to the superimposed load applied on the B2 beam, the cracking process began already in the first day of load application. Note that, in both structures cracking was not important along the beam, except in the zone near to the central support, where the bending moment is negative and the tensile stresses reach values that may cause cracks. Cracking patterns on the upper layer of concrete slab for beam B2 are shown in Fig. 12, for instance.

In Fig. 13 is shown the development of the deflection along the longitudinal axis of beams B1 and B2 for instantaneous and long-term responses. Maximum displacements took place at mid-span of each span. In Fig. 14, the computed initial and final bending moment diagrams obtained with the present model are plotted for beam B2 (the most loaded) and compared with the results of Gilbert and Bradford (1995). The instantaneous bending response (3 days) is the same in all cases; however some differences are obtained for the final period of analysis (340 days). This difference is attributed

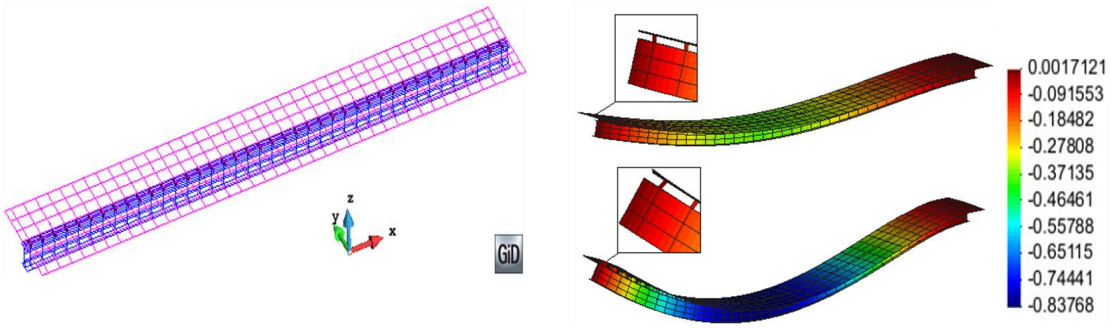

a) Finite element mesh b) Deformed mesh (cm) for 3 and 340 days

Fig. 10 Geometry and deformed mesh for composite beam B2

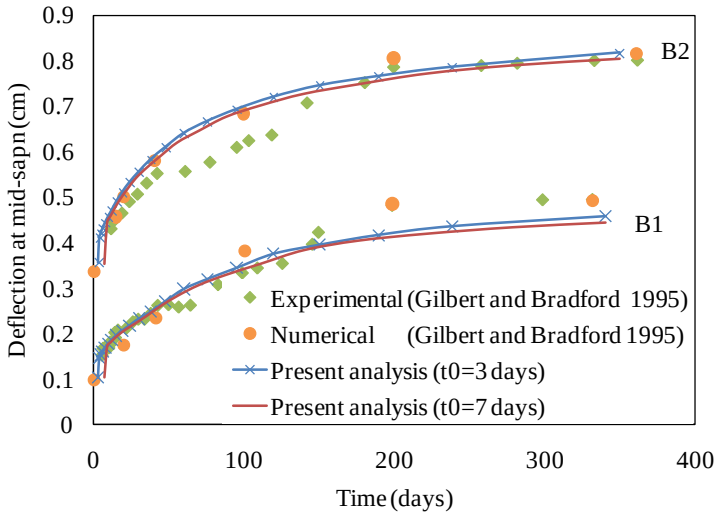

Fig. 11 Mid-span deflection for continuous steel-concrete composite beams

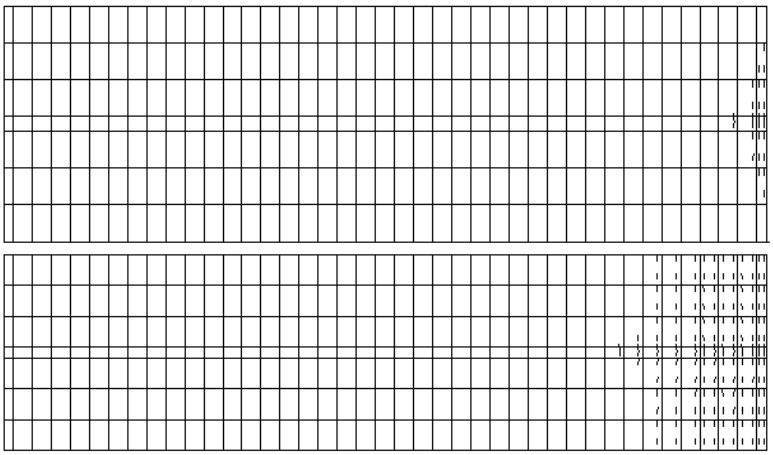

Fig. 12 Cracking evolution on the upper layer of half B2 beam for 3 and 340 days

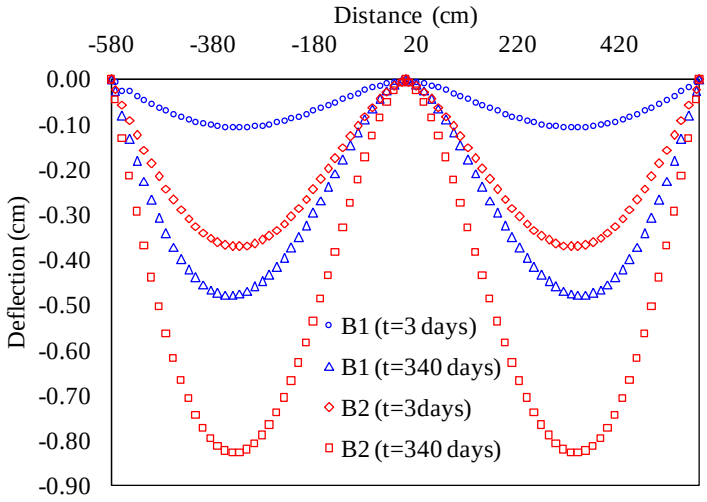

Fig. 13 Deflections along axis of the beams

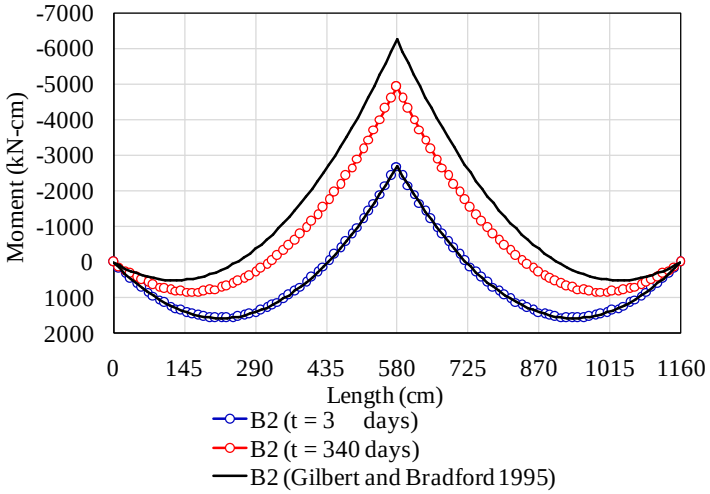

Fig. 14 Initial and final bending moment diagrams for composite beam B2

to cracking monitoring algorithm used in each model. In the cited reference the authors used a more simplified analysis neglecting the tension stiffening effect. It can be seen that the time-dependent redistribution of moments that occurs in continuos composite members at service loads due long-term effects is considerable for this particular case. More parametric studies are needed in order to give more general conclusions about this fact.

In relation to the computational time, the non-linear code took approximately 41 minutes for analyzing beams B1 and B2 despite only using 21 time steps. The analyses were carried out in the same computer used in the previous application. The current band solver needs to be improved in order to minimize the bandwidth of the system and the execution time. However, the implementation of a parallelized sparse solver seems to be a better option and the corresponding work is in progress.

7. Conclusions

Concrete long-term effects in steel-concrete composite beams were studied and implemented in this work. A computer code for short-term analysis until the structural collapse developed by Tamayo (2011) was extended in the present study to include creep and shrinkage effects (Dias 2013). Aging was introduced using the Solidification Theory. The viscoelastic behavior is represented by a rheological model applying a Kelvin chain with their elements placed in series. The Kelvin chain showed a good behavior when four or five elements were used. Parameters of the Kelvin chain were adjusted using a least squares procedure. Creep and shrinkage models of the CEB-FIP90 were able to quantify correctly the creep coefficient and the shrinkage strain for the studied examples.

The analysis considers material nonlinearity caused by cracking of the concrete slab in the negative moment regions, the time dependent deformations caused by creep and shrinkage in the concrete and the partial interaction at the slab-beam interface. Computed results were shown to be in close agreement with laboratory measurements taken on two full-scale continuous composite beams tested for a period of 340 days. Only one-dimensional numerical analyses were found in the technical literature of the topic for analyzing these two experimental composite beams. In this work, a three-dimensional numerical model which is able to consider shear lag phenomenon at the concrete slab is used. Therefore, a more accurate response and a more realistic representation of cracking patterns at the concrete slab can be obtained.

Maximum slips of connectors took place at the end of the composite beams for an analysis time of 340 days. These slips correspond to the 71% and 78% of the ultimate shear force of the connector for beams B1 and B2, respectively. Therefore, the use of a nonlinear constitutive law for the connectors is needed since the beginning of the analysis. Studies are undergoing in order to include prestressed tendons at the concrete slab for modeling long-span bridges.

Acknowledgments

The financial support provided by CAPES and CNPQ is gratefully acknowledged.

References

Alwis, W.A.M., Olorunniwo A. and Ang, K.K. (1994), "Long-term deflection of RC beams", *J. Eng.*, **120**, 2220-2226.

Bazant, Z.P. (1988), "Material models for structural creep analysis", Mathematical Modeling of creep and shrinkage of concrete, John Wiley & Sons Ltd, 99-215.

Bazant, Z.P. and Oh, B. (1984), "Deformation of progressively cracking reinforced concrete beams", *J. Am. Concrete Inst.*, **81**, 268-278.

Bazant, Z.P. and Prasannan, S. (1988), "Solidification theory for aging creep", *Cement Concrete Res.*, **18**, 923 – 932.

Chaudhary, S., Pendharkar, U. and Nagpal, A.K. (2007), "Service load behavior of continuous composite beams with precast decks considering creep, shrinkage and cracking", *Asian J. Civil Eng. (Building and housing)*, **8**(4), 423-442.

Comité Euro-International du Béton (1990) "CEB-FIP model code 1990", CEB Bull. No. 213/214, Lausanne, Switzerland; 1983.

Dias, M.M. (2013), "Numerical analysis of steel-concrete composite beams by using the finite element method:

creep and shrinkage effects over time", MSc. Dissertation, Federal University of Rio Grande do Sul, Porto Alegre (in Portuguese).

Gara, F., Leoni and G. and Dezi, L. (2009), "A beam finite element including shear lag effect for the time dependent analysis of steel-concrete composite decks", *Eng. Struct.*, **31**, 1888-1902.

Gilbert, R.L. and Bradford, M.A. (1995) "Time-dependent behavior of continuous composite beams at service loads", *J. Struct.l Eng.* , **121**, 319-327.

Hwang, J. and Kwak, H.G. (2013) "Improved FE model to simulate interfacial bond-slip behavior in composite beams under cyclic loading", *Comput. Struct.*, **125**, 164-176.

Jaccoud, J. P. and Favre, R. (1982), "Flèche des structures en béton armé - vérification expérimentale d'une méthode de calcul", Annales de I'institut Technique du Bâtiment et des Travaux Publics, Lausanne.

Jiang, M.; Qiu, W. and Zhang, Z. (2009), "Time-dependent analysis of steel-concrete composite beams" International Conference on Engineering Computation, 8-11.

Liu, X., Bradford, M.A. and Erkmen, R.E. (2013), "Time-dependent response of spatially curved steel-concrete composite members. I: computational modeling", *J. Struct. Eng.* , 1**39**, CID: 04013004.

Macorini, L., Fragiacomo, M., Amadio, C. and Izzuddin, B.A. (2006), "Long-term analysis of steel-concrete composite beams: FE modelling for effective width evaluation", *Eng. Struct.*, **28**, 1110-1121.

Povoas, R. (1991), "Non-linear models for analysis and dimensioning", Ph.D. Dissertation, Porto University, Porto (in Portuguese).

Razaqpur, A. and Nofal, M. A. (1989) "Finite element for modeling the nonlinear behavior of shear connectors in composite structures ", *Comput. Struct.*, **32**, 169-174.

Sakr, M.A. and Sakla, S.S. (2008), "Long term deflection of cracked composite beams with nonlinear partial shear interaction: I – Finite element modeling", *J. Construct. Steel Res.*, **64**, 1446-1455.

Smith, I.M., Griffiths, D.V. and Margetts, L. (2014), "Programming the finite element method", (5th Edition), John Wiley & Sons Ltd, New York, NY, United Kingdon.

Tamayo, J.L.P. (2011), "Numerical analysis of composite beams by the finite element method", MSc. Dissertation, Federal University of Rio Grande do Sul, Porto Alegre (in Portuguese).

Tamayo, J., Morsch, I. and Awruch, A.M. (2014) "Short-time numerical analysis of steel-concrete composite beams", *J. Brazil. Soc. Mech. Sci. Eng.*, DOI 10.1007/s40430-014-0237-9.

Valipour, H.R. and Bradford, M.A. (2009)," A steel-concrete composite beam element with material nonlineatities and partial shear interaction", *Finite Elem. Anal. Des.*, **45**, 966-972.

CC